THE ASTROPHYSICAL JOURNAL, 460:L11–L14, 1996 March 20

DUST-ENSHROUDED AGN MODELS FOR HYPERLUMINOUS, HIGH-REDSHIFT INFRARED GALAXIES

GIAN LUIGI GRANATO[1]
Osservatorio Astronomico di Padova, Padova, Italy
LUIGI DANESE[2]
International School for Advanced Studies
AND
ALBERTO FRANCESCHINI[3]
Dipartimento di Astronomia di Padova, Padova, Italy
Received 26 December 1995; accepted 1996 January 16

ABSTRACT

We investigate models for the power supply and broadband spectral energy distribution (SED) of hyperluminous IR galaxies, recently discovered at high redshifts, in terms of the emission from an active nucleus embedded in a torus-like dusty structure. We find consistent solutions in terms of a simple torus model extended several hundreds of parsecs, with A_V in the equatorial plane of a few hundred and a typical covering factor of over 50%. Objects as different as the prototypical high-z galaxy IRAS F10214, the $z = 0.93$ IR object IRAS F15307, IRAS 09104, found in a high-z cooling flow, and the optically selected broad absorption line "Cloverleaf" quasar, are all fitted by the same solution for decreasing values of the polar angle to the line of sight and proper scaling of the luminosities. We suggest that such luminous, high-z IR objects are heavily buried quasars surrounded by large amounts of dust with high covering factors and large optical depths. Comparison with ultraviolet-excess QSOs suggests that they are observed during a transient phase. Forthcoming observations in the far-IR will soon allow probing of this phase and its relationship with the—possibly concomitant—formation of the nuclear black hole and the host galaxy.

Subject headings: dust, extinction — galaxies: active — galaxies: ISM — galaxies: nuclei — gravitational lensing — infrared: galaxies

1. INTRODUCTION

A new class of peculiar hyperluminous IR galaxies ($L_{IR}/L_\odot > 10^{12}\ h^{-2}$, for $q_0 = 0.5$ and $h = H_0/100$ km s^{-1} Mpc^{-1}) has recently been discovered at moderate to high redshifts. They appear to have fairly similar luminosities, in particular now that the most extreme example, IRAS F10214, at $z = 2.286$ with an observed $L_{IR} \sim 3 \times 10^{14}\ h^{-2}\ L_\odot$, has been proved to be significantly amplified by a foreground gravitational lens (see, e.g., Broadurst & Lehar 1995). Other well-studied hyperluminous IR objects are IRAS F15307 ($z = 0.93$ and $L_{IR} \sim 1 \times 10^{13}\ h^{-2}\ L_\odot$) and IRAS 09104+4109 ($z = 0.442$ and $L_{IR} \sim 6 \times 10^{12}\ h^{-2}\ L_\odot$).

While the Cloverleaf is definitely a QSO, the presence of an active nucleus in the other three objects is supported by various observations, including strong emission lines typical of local type 2 active galactic nuclei (AGNs) (see, e.g., Soifer et al. 1995), the optical-UV polarization (see, e.g., Hines et al. 1995), and, concerning in particular IRAS F10214, the severe constraints on the size of the source (Eisenhardt et al. 1996) and the recently discovered broad emission lines in polarized light (Miller 1995).

Quite an impressive comparison has been recently suggested by Barvainis et al. (1995) between the overall spectrum of IRAS F10214 and that of the radio-quiet, broad absorption line Cloverleaf quasar at $z = 2.558$, which has a spectrum identical to that of IRAS F10214 in the IR/submillimeter but is 2 orders of magnitude brighter in the optical. This is suggestive that IRAS F10214 and the Cloverleaf might be the high-redshift and high-power counterparts of narrow- and broad-line AGNs, respectively. The only difference between the two would be in the line of sight, intersecting a torus-like distribution of gas and dust in the former while falling close to the almost clean polar cap in the latter.

However, published fits to the IR spectra in terms of emission from dust illuminated by a luminous AGN fail to reproduce the observed broad dust emission spectra in the rest-frame 10–500 μm band for all such objects.

This Letter is mainly devoted to showing quantitatively that the emission of a dusty torus–like structure dominates the observed IR spectra of hyperluminous IR galaxies harboring a bona fide active nucleus. We use the radiative transfer code developed by Granato & Danese, which successfully fits the available data on both broad- and narrow-lined local AGNs (Granato & Danese 1994; Granato, Danese, & Franceschini 1996). The possible effects of gravitational lensing in modifying the shape of the spectral energy distributions (SEDs) is properly taken into account. The relationship among IR and optically selected AGNs is also discussed.

2. THE TORUS MODEL

A thorough discussion of our adopted dust-torus model and the numerical method developed to compute the emitted SED can be found in Granato & Danese (1994). Only its basic features are summarized here.

[1] Osservatorio Astronomico, Vicolo dell'Osservatorio 5, I-35122 Padova, Italy; granato@astrpd.pd.astro.it.
[2] International School for Advanced Studies, Strada Costiera 11, I-34014 Trieste, Italy; danese@astrpd.pd.astro.it.
[3] Dipartimento di Astronomia, Vicolo Osservatorio 5, I-35122, Padova, Italy; franceschini@astrpd.pd.astro.it.

The code solves, through an iterative numerical scheme, for the transfer equation of the radiation that originates from the central optical-UV source in an axisymmetric dust distribution. The dust is composed of a mixture of grains, in thermal equilibrium with the radiation field, and extends out to a maximum radius r_{max}. We adopted the six-silicate and graphite grain model described by Rowan-Robinson (1986), which fits reasonably well the average galactic absorption law. The inner boundary of the cloud, r_{min}, is set by the sublimation of all species of grains, which is assumed to happen at temperatures of 1500 K for graphite and 1000 K for silicate grains.

To keep the number of free model parameters to a minimum, we have adopted a dust density distribution that is constant with radial distance from the central source and a function of the polar angle Θ only:

$$\rho(\Theta) = C \exp(-\gamma \cos^2 \Theta) \quad (1)$$

for $r_{min} \leq r \leq r_{max}$. This allows directions close to the poles of the distribution to be less affected by dust extinction (the classical torus configuration). Such optically thin dust along the axis scatters a fraction (on the order of a few percent) of the primary spectrum into orthogonal directions, producing a highly polarized "secondary" spectrum. This distribution is then parameterized by the three constants C, r_{max}/r_{min}, and γ, where the normalization C is conveniently replaced by the equatorial optical thickness τ_e of the cloud at 0.3 μm ($A_V \simeq 0.61\tau_e$ and, assuming a standard dust-to-gas ratio, $N_H \simeq 1.2 \times 10^{21} \tau_e$ cm^{-2}).

As for the input blue-bump spectra, we employ a functional description consisting of a broken power law with $\alpha = -0.5$ for $\log \nu < 15.4$, $\alpha = -1.0$ for $15.4 \leq \log \nu < 16$, and a sharp cutoff with $\alpha = -2.2$ for $\log \nu \geq 16$. This provides a good approximation of the observed optical-UV portion of the blue bump and is consistent with indications from observations of high-z objects, photoionization models for the emission lines, and computations of accretion disk spectra for the EUV regime.

3. MODEL SPECTRAL ENERGY DISTRIBUTIONS VERSUS DATA

Fits to the observed millimeter-IR-UV SEDs of the Cloverleaf, IRAS F10214, IRAS 09104, and IRAS F15307 are shown in Figure 1. The *same* model with $\tau_e = 250$, $r_{max}/r_{min} = 500$, and $\gamma = 6.2$ is shown here to account remarkably well for all objects, when observed from different viewing angles.

3.1. *IRAS F10214+4724 and the Cloverleaf*

The SED of the Cloverleaf is reproduced if the torus is observed close to the pole, while that of IRAS F10214 is when it is seen along the equator, provided that the latter SED is scaled upward in luminosity by a factor of 2.

The analysis of the Cloverleaf and IRAS F10214 is complicated, however, by the fact that they are gravitationally lensed objects. For a given lens geometry, the lensing magnification m depends on the source's size and surface brightness distribution. Since the emission in different spectral regimes arises from regions of different sizes, not only the normalization but also the shape of the SED could be affected. In particular, in our tori the extension of the emission usually, but not always, increases with λ. The surface brightness distribution is, in any case, rather complex and heavily dependent on the line of sight and observation wavelength.

We show in Figure 2 contour maps of the model for an edge-on line of sight at four representative wavelengths. For such an equatorial view, the observed emission of our torus configuration would be rather extended at any wavelength. At far-IR wavelengths, the system is optically thin and extends to r_{max}. In the near-IR, the hot inner dust is heavily obscured while the relatively weak optical-UV continuum consists of photons initially escaping along directions close to the polar axis, where the optical thickness is low, and then scattered along our line of sight by dust in the polar region.

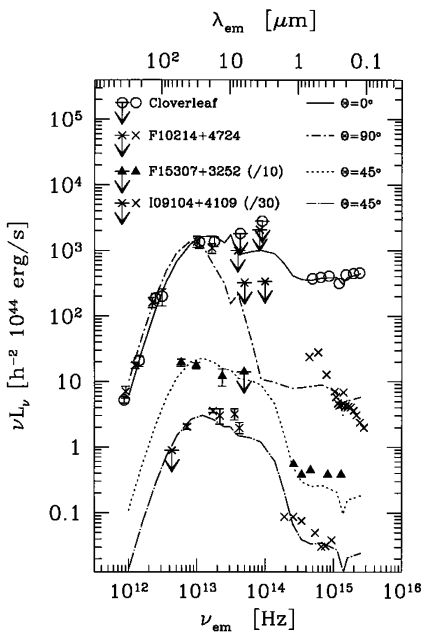

FIG. 1.—A *simultaneous* fit of the dust-enshrouded QSO model to the rest-frame SEDs of the four hyperluminous IR sources. The dusty torus has an equatorial optical thickness at 3000 Å of $\tau_e = 250$ ($A_V = 150$), the ratio between the outer and inner radii is 500, and the density depends only on the polar angle (see eq. [1]), so that at the pole $\tau_p = 0.50$. IRAS F10214 and the Cloverleaf correspond to an equatorial and polar viewing angle, respectively. The SEDs of IRAS F15307 and IRAS 09104, downscaled in the figure by factors of 10 and 30, respectively, to avoid confusion, are reasonably well reproduced by the *same* model, but viewed from $\Theta \simeq 45°$ and conveniently scaled in luminosity.

On the contrary, when the model is observed from a direction with moderate line-of-sight extinction (pole-on view), we see directly the near-IR emission from the hot dust, as well as the primary source. The emission then becomes more and more compact at decreasing wavelengths.

We have performed a detailed modeling of the lensing geometry for different lines of sight. The basic results on the chromatic effects of the lensing are summarized here, while for the full treatment we defer to Granato et al. (1996).

Though uncertain, the lensing geometries for the Cloverleaf and IRAS F10214 are clearly much different. In the former case, the observed quadruple image is explained by putting the source well inside the tangential diamond caustic, where the magnification is on the order of a few times, with a small gradient. It is weakly dependent on the source's size as long as it remains inside the caustics and relatively far from the cusps. Thus, despite the strong wavelength dependence of the torus, when observed from the pole, we find that the predicted magnification is achromatic to within 20%.

For two independent reasons, one related to the complex source geometry (see Fig. 2) and the other to the source's

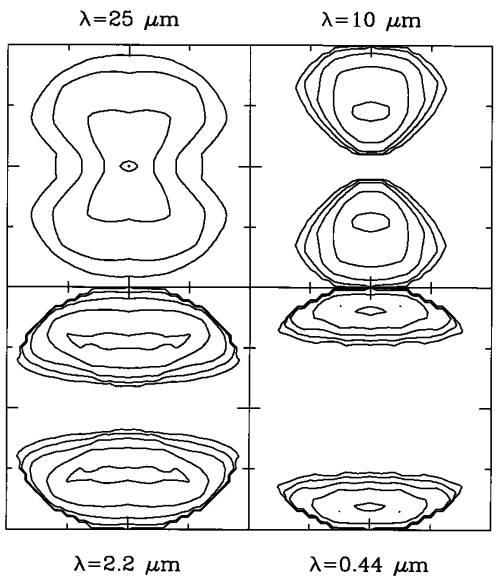

FIG. 2.—Brightness contours at four different wavelengths of the circumnuclear dust distribution used to reproduce the SEDs of the Cloverleaf and hyperluminous IRAS galaxies. In this case the "torus" is seen edge-on, i.e., $\theta = 90°$. The boxes have a width of $2r_{max}$, and the levels refers to 0.01, 0.03, 0.1, 0.3, and 0.9 of the peak brightness.

position with respect to the diamond caustic, the case of IRAS F10214 is more intricate. The arc observed in the *K* band and optical may be explained by centering the source just outside a cusp of the diamond. In this region, the amplification is large and has a large gradient. Given the noncircular source symmetry, the magnification also depends on the angle α between the torus axis in Figure 2 and that of the diamond caustic in the plane of the sky.

Thus, any solution for the lensing geometry and chromatics of IRAS F10214 is model-dependent to some extent. If we adopt the lens solution of Broadhurst & Lehar (1995) and the torus model of Figure 2, we find an average magnification factor of $m \simeq 15$ and chromatic distortions of the SED within a factor of 3. A *Hubble Space Telescope* image of IRAS F10214 taken at 0.8 μm by Eisenhardt et al. (1996) provides strong support to the gravitational-lensing hypothesis. The arc is unresolved in the transverse direction, giving a direct upper limit to the radius of the UV source of $\sim 150\, h^{-1}$ pc, consistent with our inferred value of $\sim 100\, h^{-1}$ pc for our UV model source (see Fig. 2). On the other hand, Eisenhardt et al.'s values for the total magnification, $m \simeq 100$, and for the UV source size, $20\, h^{-1}$ pc, inferred indirectly from the flux ratio of the arc to the counterimage, are made uncertain by differential extinction, time delays, and microlensing along the two light paths. They also estimated a magnification of a factor of ~30 for the IR emission.

Although these two models predict different magnification on very small scales, they nevertheless agree that the effect of the lensing in changing the ratio of the optical to far-IR luminosities is within a factor of 3. The main effect would be on the relative normalization of the IR and the optical-UV spectrum in Figure 1, which however could be easily accounted for with small changes in the equatorial optical thickness and/or viewing angle.

3.2. *IRAS F15307 and IRAS 09104*

The lack of submillimeter observations leaves the SEDs for these two sources less well defined. However, it is interesting to note that the same model, conveniently downscaled in luminosity, also provides a reasonable fit to these data when observed from an intermediate angle, $\Theta \simeq 65°$ (Fig. 1).

Obviously, fit parameters for individual sources are rather poorly constrained (e.g., r_{max}/r_{min} can be changed to 800 and 300, respectively, and an interplay between the viewing angle and τ_e is allowed). However, additional observations help to better understand these objects. Hines et al. (1995) inferred an intrinsic spectrum of IRAS F15307 remarkably similar to that of a "typical" QSO, with a luminosity in close agreement with our model value (see Table 1). In our configuration, the optical-UV photons are yielded by scattering of the intrinsic spectrum by dust grains, which is responsible for the observed polarization (cf. Hines et al. 1995).

High polarization is also observed in IRAS 09104 (Hines & Wills 1993). The stellar continuum is important here longward of 0.45 μm (rest frame) and dilutes the observed polarization (Hines & Wills 1993; Kleinmann et al. 1988). After correction for starlight, we are left with an $F \propto \nu^{-0.6}$ continuum with an absolute magnitude close to the value required by the model. The predicted polarization is also close to the the observed values provided that dilution at a level of 30%–50% by stellar light is taken into account.

4. DISCUSSION

The observed SEDs of the four hyperluminous IR objects are consistent with the presence of dust distributions that encompass $\sim 10^7\ M_\odot$ around a luminous AGN, with $A_V \simeq 100$–300 over 50% or more of the nuclear sky, r_{max}/r_{min} of several hundred, and a fraction of the remaining sky (the "cones") containing more diffuse matter that scatters some of the primary continuum into our line of sight. Further information on our best-fit solutions is provided in Table 1.

More compact and thicker tori, as proposed by Pier &

TABLE 1

MODEL SOLUTIONS

Object	$L_{bb,46}$	r_{min} (pc)	r_{max} (pc)	M_d ($M_\odot$)
Cloverleaf.....	$22m^{-1}\, h^{-2}$	$2.3m^{-1/2}\, h^{-1}$	$1170m^{-1/2}\, h^{-1}$	$3.5 \times 10^7 m^{-1}\, h^{-2}$
IRAS F10214.....	$40m^{-1}\, h^{-2}$	$3.2m^{-1/2}\, h^{-1}$	$1580m^{-1/2}\, h^{-1}$	$6.4 \times 10^6 m^{-1}\, h^{-2}$
IRAS F15307.....	$4.0\, h^{-2}$	$1.0\, h^{-1}$	$500\, h^{-1}$	$6.4 \times 10^6\, h^{-2}$
IRAS 09104.....	$1.6\, h^{-2}$	$0.6\, h^{-1}$	$316\, h^{-1}$	$2.6 \times 10^6\, h^{-2}$

NOTE.—Model solutions for the bolometric luminosity of the primary optical-UV continuum $L_{bb,46}$ in units of 10^{46} ergs s^{-1} Hz^{-1}, the inner (r_{min}) and outer (r_{max}) radii of the dust torus, and total dust mass involved. For the two lensed objects, all quantities depend on the assumed magnification factor *m*, likely to be $\gtrsim 10$ for IRAS F10214 and ~3 for the Cloverleaf.

Krolik (1992) in a different context, would produce quite different SEDs, with pronounced peaks at 8–10 μm quickly falling at longer λ for nearly face-on objects. For instance, a torus model with their standard values of the parameters ($r_{max}/r_{min} \lesssim 10$ and $\tau_e \gtrsim 1000$) would predict a falloff of the SED (in νL_ν) by more than 2 orders of magnitude from the peak down to 100 μm, whereas the Cloverleaf exhibits a rather flat spectrum up to ~30 μm with a decrease of less than a factor of 10 at 100 μm (see Fig. 1). In the case of sources viewed at large polar angles, the compact and very thick tori proposed by Pier & Krolik would produce narrow spectra, peaking at ~10–15 μm (while the spectra reported in Fig. 1 exhibit maxima at ~30–40 μm) and with too-steep falloffs both at longer and shorter wavelengths. A detailed comparison of various torus models may be found in Granato & Danese (1994).

An interesting step would now be to understand if this sample of hyperluminous objects could be interpreted as just the optically thick population viewed edge-on in a unified picture of quasar activity, where the common ultraviolet excess (UVX)–selected objects are the pole-on, optically thin counterparts. A clue to this question may come from a comparison of the Cloverleaf's overall spectrum with those of UVX QSOs and Seyfert 1 nuclei, as reported in Figure 3.

We see here that the average IR-to-optical luminosity ratio of Seyfert 1's is greater by a factor of 2–3 than the same for UVX QSOs, a fact that may be interpreted as an effect of the nuclear luminosity on the environment, producing a decreasing dust covering factor and/or optical depth at increasing luminosity. We also see that the Cloverleaf is at variance with respect to this picture, because its IR-to-optical luminosity ratio is even higher than that of low-luminosity Seyfert 1 nuclei.

Our model fits to the data summarized in Figure 3 may be characterized, for example, by the equatorial optical thickness, τ_e, of the dust torus. A typical SED of high-luminosity UVX QSOs is fitted by values in the range $5 < \tau_e < 15$; for lower luminosity Seyfert 1's, Granato & Danese (1994) found $10 < \tau_e < 40$, while for NGC 1068, $50 \lesssim \tau_e \lesssim 100$. For the Cloverleaf and the other hyperluminous IR objects we find here $100 < \tau_e < 500$. Our conclusion is that the latter class of AGNs is strongly at variance with respect to the other, usual UVX AGNs, not only because of the very high inferred values of τ_e but also because of their very high nuclear luminosities, which breaks down the trend for a lower coverage at higher luminosities.

Note, finally, that the Cloverleaf exhibits broad absorption lines in the spectrum, a situation that may arise from radiation-pressure acceleration of material in the torus polar regions for very high, possibly super-Eddington, accretion rates. All this is

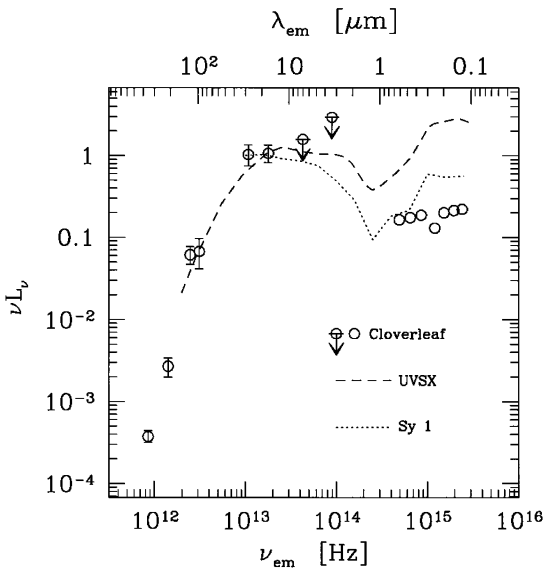

FIG. 3.—Comparison of the average broadband spectra for various AGN classes. UVX QSOs (Elvis et al. 1994) appear as a dashed line, and Seyfert 1 nuclei (Granato & Danese 1994) as a dotted line. SED data on the Cloverleaf are from Barvainis et al. (1995). The SEDs have been normalized at 18 μm.

suggestive of a possible initial transient phase of formation of a supermassive black hole, when the gas is still very abundant around the nucleus.

How does this phase relate with that of formation of the host galaxy? The detection of a large amount of CO in IRAS F10214 may indicate that star formation is an ongoing process in the host galaxy. Also, the detection of dust in the submillimeter range for a few high-z quasars may be in agreement with the idea of an initial phase in which a "young" nucleus is immersed in a "young" galaxy with large amounts of gas not yet locked into stars.

Any conclusion is obviously premature until good enough statistics are available on this class of sources. The forthcoming *Infrared Space Observatory* (*ISO*) mission is expected to improve this situation substantially, given its dramatic sensitivity improvement with respect to *IRAS*. We estimate that on the order of 10^3 UVX AGNs will be discovered in the foreseen 25 deg^2 sky area covered by various *ISO* surveys at $\lambda \simeq 5$–100 μm. The dusty QSOs that will be found, whose number is unpredictable now since we do not know the duration of the dust-enshrouded phase, will cast light on the quasar formation process and its relationship with that of the host galaxy.

We are indebted to G. De Zotti for critical reading of the paper and fruitful discussions.

REFERENCES

Barvainis, R., Antonucci, R., Hurt, T., Coleman, P., & Reuter, H.-P. 1995, ApJ, 451, L9
Broadhurst, T., & Lehar, J. 1995, ApJ, 450, L41
Eisenhardt, P. E., Armus, L., Hogg, D. W., Soifer, B. T., Neugebauer, G., & Werner, M. W. 1996, ApJ, in press
Elvis, M., et al. 1994, ApJS, 95, 1
Granato, G. L., & Danese, L. 1994, MNRAS, 268, 235
Granato, G. L., Danese, L., & Franceschini, A. 1996, in preparation
Hines, D. C., Schmidt, G. D., Smith, P. S., Cutri, R. M., & Low, F. J. 1995, ApJ, 450, L1
Hines, D. C., & Wills, B. J. 1993, ApJ, 415, 82
Kleinmann, S. G., Hamilton, D., Keel, W. C., Wynn-Williams, C. G., Eales, S. A., Becklin, E. E., & Kuntz, K. D. 1988, ApJ, 328, 161
Miller, J. S. 1995, talk presented at Natl. Acad. Sci. Colloq., Quasars and AGN, High-Resolution Radio Imaging (1995 March 24–25, Irvine, CA)
Pier, E. A., & Krolik, J. H. 1992, ApJ, 401, 99
Rowan-Robinson, M. 1986, MNRAS, 219, 737
Soifer, B. T., Cohen, J. G., Armus, L., Matthews, K., Neugebauer, G., & Oke, J. B. 1995, ApJ, 443, L65